scientific reports

Check for updates

OPEN

Numerical study on fractional order nonlinear SIR-SI model for dengue fever epidemics

Lalchand Verma[1,2], Ramakanta Meher[2], Omid Nikan[3]✉ & Akeel A. Al-Saedi[4]

This paper focuses on a combined SIR-SI epidemic model to evaluate the transmission dynamics of dengue fever, integrating the susceptible-infected-recovered (SIR) framework for the human population with the susceptible-infected (SI) framework for mosquitoes. The model is formulated as a system of nonlinear differential equations and is further extended by incorporating fractional-order derivatives in the Caputo sense to capture memory effects in disease transmission. A thorough investigation of the disease-free and endemic equilibrium points is conducted, encompassing both local and global stability at the disease-free state. The basic reproduction number, R_0, is derived, and a sensitivity analysis is performed to identify the key parameters influencing the transmission dynamics. To ensure mathematical rigor, the existence and uniqueness of the model's solutions are also examined. For numerical approximation, the two-step Lagrange polynomial method is applied, enabling simulation of the model under various fractional orders and parameter settings. The results demonstrate that the fractional-order approach offers deeper insights into the dynamics of dengue transmission, highlighting the importance of memory effects. These findings provide valuable guidance for medical professionals, policymakers, and public health authorities in designing more effective control strategies.

Keywords Caputo fractional derivative, SIR-SI dengue epidemic model, Fractional differential equations

Dengue fever represents a major public health concern worldwide, placing considerable strain on medical infrastructures and economic resources, ultimately leading to increased rates of hospitalization and death. The symptoms usually manifest within three to fourteen days after infection and may include severe headaches, high fever, nausea, muscle and joint pain, as well as a distinctive skin rash accompanied by itching. Most individuals recover from dengue fever within two to seven days[1]. According to the World Health Organization, the following key facts about dengue have been reported[2,3]:

- Dengue fever is caused by a mosquito infected with the dengue virus, which is transmitted to humans through mosquito bites.
- Between 100 and 400 million cases are reported annually, meaning nearly half of the world's population is at risk.
- Urban and semi-urban areas in tropical and subtropical climates are the most common locations where the disease is found.
- There is no specific treatment available for dengue or severe dengue.

Mathematical modeling is crucial for managing epidemics and implementing preventive measures. This study analyzes infection and recovery rate statistics, utilizing several mathematical models established in recent decades to enhance understanding and predictions. Examples include the simultaneous outbreak of dengue and COVID-19 in Brazil[4], the interaction between Zika and Dengue with cross-enhancement effects[5], and a fractional-order model incorporating quarantine and vaccination strategies for dengue transmission[6]. A well-known framework for studying disease spread is the susceptible-infected-recovered (SIR) model, first proposed in[7]. Additional models have been examined, including the SIR model with constant human and vector

[1]Department of Applied Sciences and Humanities, Panipat Institute of Engineering and Technology, Samalkha, Panipat, Haryana 132102, India. [2]Department of Mathematics, Sardar Vallabhbhai National Institute of Technology, Surat, Surat, Gujarat 395 007, India. [3]School of Mathematics and Computer Science, Iran University of Science and Technology, Narmak, Tehran 16846-13114, Iran. [4]Department of Mathematics, College of Education, Misan University, Misan 62001, Iraq. ✉email: omidnikan77@yahoo.com

populations, as well as the susceptible-exposed-infected-recovered (SEIR) model, specifically developed for studying the impact of rainfall on the spread of dengue in Thailand[8]. Supriatna et al.[9] analyzed the SIR-SI model, incorporating age-dependent survival rates, effectively describing dengue transmission dynamics between humans and mosquitoes. The authors discussed comparing the Wolbachia strategy and vaccination, highlighting the potential of combining or prioritizing biological interventions for controlling dengue.

Fractional calculus is currently a popular and emerging area of study[10–13]. The research conducted in this newly established study topic has been published in prestigious journals, seminars, workshops, and international conferences, showcasing its high quality and demonstrating its potential and practicality. The study is motivated by the extensive application of fractional calculus in several engineering and science fields. Prominent mathematicians such as Fourier, Liouville, Euler, and Riemann made significant contributions to classical calculus during the 18th century, which were documented in the literature. Moreover, that specific era was widely recognized as the pinnacle of fractional calculus, during which numerous significant breakthroughs were achieved. Fractional calculus remains a subject of great interest among scholars, primarily due to its extensive range of practical applications. Fractional calculus has been employed in mathematical modelling to elucidate diverse inherent phenomena and retrieve measurements that classical calculus cannot represent. Furthermore, because of the localized nature of its fractional differential operator, fractional calculus exhibits a greater level of freedom compared to classical calculus. Recent research has developed fractional models, such as a generalized HBV model that captures both transmission channels, an HBV model with cell-to-cell and virus-to-cell transmissions and adaptive immunity, and a two-strain SVLIR model with vaccination and quarantine[14–16].

In recent years, numerous studies have focused on integer-order and fractional derivatives, incorporating both local and non-local kernels across various mathematical models[17–19]. Hamdan and Kilicman[20] investigated the SIR epidemic model for dengue transmission using a fractional methodology. Hamdan and Kilicman[21] used the fractional derivative to discuss the mathematical model of dengue using the real data of Malaysia. Hoang et al.[22] analyzed the dynamics and numerical approximations of a fractional-order susceptible-infected-susceptible epidemic model incorporating a saturating contact rate. Ahmad et al.[23] conducted an analysis of a fractional dengue model that provides a description of the dynamics of dengue. This model incorporates interactions between human populations and vector populations, specifically mosquito populations, with the aim of improving understanding and forecasting epidemics. Harris[24] analyzed the SIR model to analyze COVID-19's Omicron surge in New York City, using least-squares minimization to estimate infection dynamics, improving epidemic forecasting and public health response strategies. Contreras et al.[25] have presented a comprehensive multi-group SEIRA model to depict the transmission of COVID-19 throughout a heterogeneous population and have evaluated it using a numerical case study. Ortiz et al.[26] have examined the particular to a nation forecasting model for the effective reproduction number R_t of Coronavirus health issues.Several studies have contributed to the modeling of COVID-19 dynamics using advanced mathematical tools, including a correlated stochastic epidemic model incorporating vaccination, an optimal control-based epidemiological model for analyzing pandemic trends, and a fractional-order model for asymptotic analysis of the disease transmission[27–29]. Sapakova et al.[30] evaluated the SIR model to assess the epidemiological situation in Kazakhstan and neighboring countries, using real data to analyze transmission dynamics and intervention impacts. Mungkasi[31] investigated an enhanced variational iteration approach to address the SIR model for dengue fever, addressing its application to disease dynamics in South Sulawesi for improved predictions. Shah et al.[32] examined a fractional model of dengue fever utilizing the Caputo-Fabrizio derivative. Vijayalakshmi and Ariyanatchi[33] studied the fractional dengue fever model in the ABC sense and analyzed the stability of the proposed model. Numerous researchers have explored various epidemic models incorporating fractional derivatives, aiming to solve these fractional models through numerical methods such as Jan and Boulaaras[34] evaluated the fractional-order dynamics of dengue infection, utilizing nonlinear incidence functions to provide a more refined model of the disease's transmission dynamics. Maayah et al.[35] studied the numerically solve the fractional order of the SIR model of dengue fever using the Laplace transform method. Ahmad et al.[36] discussed the stability analysis of the transmission of Buruli diseases through the fractional SIR model with the application in a bio-medical. Nisar et al.[37] discussed the disease's different types of mathematical models in a fractional order. Sabir et al.[38] implemented artificial neuron networks in conjunction with the Levenberg-Marquardt backpropagation to conduct a study on the numerical studies of a fractional nonlinear dengue model. Meetei et al.[39] presented a quantitative analysis utilizing the Caputo-Fabrizio fractional-order derivative to investigate dengue's transmission dynamics. Youssef et al.[40] examined the stability of SIR, SEIR, SIR-SI, and SEIR-SI models, analyzing them under the assumption that recovered patients may experience reinfection with dengue.

This research primarily aims to characterize the dynamic transmission of the dengue fever model through the SIR-SI framework using the Caputo fractional derivative. Further, we investigate the stability and reproduction number of the fractional SIR-SI model and also discuss the sensitivity analysis of the parameter. The numerical method uses the two-step Lagrange polynomial technique to solve the proposed fractional model. It also discusses the effect of distinct values of fractional order and parameters on the behaviour of the proposed model.

The structure of the paper is as follows: "Mathematical model" presents the fractional SIR-SI model for dengue fever using the Caputo derivative. "Stability analysis" and "Existence and uniqueness conditions of solution" discuss the stability analysis as well as the uniqueness and existence of the approximate solution of the proposed model, respectively. "Numerical procedure of SIR-SI model" and "Sensitivity analysis of the parameters" explain the numerical procedure of the SIR-SI model and the sensitivity analysis of the parameter, respectively. "Numerical results and discussion" provides the results and discussion. Finally, "Conclusion" presents the concluding remark of the research paper.

Mathematical model

We examine the SIR-SI epidemic model[41,42], which is a model that integrates two distinct frameworks in this section. The modeling framework includes of an SIR structure for the human population and an SI structure for the mosquito population. In this framework, the human population is divided into three compartments: susceptible (S_h), infected (I_h), and recovered (R_h) individuals. Likewise, the mosquito population is divided into two compartments: susceptible (S_v) and infected (I_v). It is further assumed that the total populations of both humans and mosquitoes remain constant over time, as reflected in the following equations.

$$N_h = S_h(t) + I_h(t) + R_h(t), \tag{1}$$

and

$$N_v = S_v(t) + I_v(t). \tag{2}$$

At the time t, $S_h(t)$ denotes the numbers of susceptible, $I_h(t)$ denote the numbers of infected and $R_h(t)$ denote the numbers of recovered humans, respectively, whereas $S_v(t)$ indicate the numbers of susceptible and $I_v(t)$ indicate the numbers of infected mosquitoes. The integrated model is expressed as a set of nonlinear differential equations representing the transmission dynamics between people and mosquitoes. Figure 1 illustrates the mathematical structure of the SIR-SI model for dengue fever.

Begin with SIR model for human population by considering death and birth quality rate in the human population[41,42]:

$$\left.\begin{aligned} \frac{dS_h(t)}{dt} &= \alpha_h N_h - \frac{d\delta_h}{N_h} I_v(t) S_h(t) - \alpha_h S_h(t), \\ \frac{dI_h(t)}{dt} &= \frac{d\delta_h}{N_h} I_v(t) S_h(t) - (\alpha_h + \beta_h) I_h(t), \\ \frac{dR_h(t)}{dt} &= \beta_h I_h(t) - \alpha_h R_h(t), \end{aligned}\right\} t \geq 0. \tag{3}$$

Subject to initial condition of the model (3) about $t = 0$ as

$$S_h(0) = S_{h_0},\ I_h(0) = I_{h_0},\ \text{and}\ R_h(0) = R_{h_0}. \tag{4}$$

On the other hand, the SI model for mosquito population after the considering death and birth quality rate in the mosquito population[41,42]:

$$\left.\begin{aligned} \frac{dS_v(t)}{dt} &= \alpha_v N_v - \frac{d\delta_v}{N_v} I_h(t) S_v(t) - \alpha_v S_v(t), \\ \frac{dI_v(t)}{dt} &= \frac{d\delta_v}{N_h} I_h(t) S_v(t) - \alpha_v I_v(t), \end{aligned}\right\} t \geq 0. \tag{5}$$

Subject to initial condition of the model (5) about $t = 0$ as

$$S_v(0) = S_{v_0}\ \text{and}\ I_v(0) = I_{v_0}. \tag{6}$$

Using Eqs. (1), (2), (3), (4), (5), and (6), the SIR and SI epidemic models are combined to form the SIR-SI dengue fever epidemic model as follows:

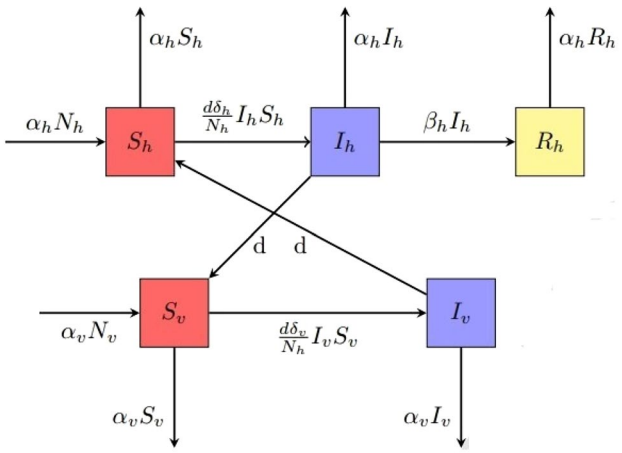

Fig. 1. The representation of SIR-SI dengue fever model.

$$\left.\begin{aligned}\frac{dS_h(t)}{dt} &= \alpha_h N_h - \frac{d\delta_h}{N_h} I_v(t) S_h(t) - \alpha_h S_h(t),\\ \frac{dI_h(t)}{dt} &= \frac{d\delta_h}{N_h} I_v(t) S_h(t) - (\alpha_h + \beta_h) I_h(t),\\ \frac{dI_v(t)}{dt} &= \frac{d\delta_v}{N_h} I_h(t) S_v(t) - \alpha_v I_v(t),\end{aligned}\right\} t \geq 0. \tag{7}$$

Subject to initial condition of the model (7) about $t = 0$ as

$$S_h(0) = S_{h_0},\ I_h(0) = I_{h_0},\ \text{and}\ I_v(0) = I_{v_0}. \tag{8}$$

In what follows, Table 1 provides the definitions of the parameters used in the model given by Eq. (7), along with their associated units.

where, the unit of $\alpha_h,\ \alpha_v,\ \delta_h,\ \delta_v$ and β_h are per day. Now, we non-dimensionalize the model (7) using the following values:

$$x(t) = \frac{S_h(t)}{N_h},\ y(t) = \frac{I_h(t)}{N_h},\ \text{and}\ z(t) = \frac{I_v(t)}{N_v}. \tag{9}$$

By substituting Eq. (9) into Eq. (7), the following system is derived:

$$\left.\begin{aligned}\frac{dx(t)}{dt} &= \alpha(1 - x(t)) - \beta z(t) x(t),\\ \frac{dy(t)}{dt} &= \beta z(t) x(t) - \gamma y(t),\\ \frac{dz(t)}{dt} &= \delta y(t)(1 - z(t)) - \mu z(t),\end{aligned}\right\} t \geq 0. \tag{10}$$

Subject to initial conditions of the model (10) about $t = 0$ as

$$x(0) = x_0,\ y(0) = y_0,\ \text{and}\ z(0) = z_0. \tag{11}$$

Where $x(t)$, $y(t)$, and $z(t)$ represent the number of susceptible humans, infectious humans, and infectious mosquitoes, respectively, at time t. $\alpha = \alpha_h,\ \beta = \frac{d\delta_h N_v}{N_h},\ \gamma = (\alpha_h + \beta_h),\ \delta = d\delta_v,$ and $\mu = \alpha_v$ are positive parameters.

The formulation of the model (7) is within integer-order derivatives. We extend the model (7) with fractional-order derivatives, providing a more general and flexible approach to describe the dynamics. Now, the fractional SIR-SI dengue fever model is

$$\left.\begin{aligned}{}_0D_t^{\kappa} x(t) &= \alpha(1 - x(t)) - \beta z(t) x(t),\\ {}_0D_t^{\kappa} y(t) &= \beta z(t) x(t) - \gamma y(t),\\ {}_0D_t^{\kappa} z(t) &= \delta y(t)(1 - z(t)) - \mu z(t),\end{aligned}\right\} t \geq 0. \tag{12}$$

The initial conditions of the model (12) are the same as in Eq. (11). To extend the model into the fractional domain, we introduce the Caputo fractional derivative, offering a more adaptable framework for capturing memory and hereditary characteristics in the context of disease transmission dynamics. The fractional order $\kappa \in (0, 1]$ governs the extent of nonlocality in the model. The Caputo fractional derivatives of $x(t)$, $y(t)$, and $z(t)$ are given by ${}_0D_t^{\kappa} x(t)$, ${}_0D_t^{\kappa} y(t)$, and ${}_0D_t^{\kappa} z(t)$, respectively. Among the various definitions of fractional derivatives, the Caputo derivative is widely used, particularly in applied modeling, because it naturally incorporates traditional

Parameter	Description	Units
α_h	Human birth/death rate	day^{-1}
α_v	Mosquito birth/death rate	day^{-1}
b	Avg. mosquito biting rate	$\text{bites mosquito}^{-1}\text{day}^{-1}$
δ_h	Human force of infection	day^{-1}
δ_v	Mosquito force of infection	day^{-1}
β_h	Human recovery rate	day^{-1}

Table 1. A detailed description of the parameters used in the model (7), along with their corresponding units.

initial conditions, making it more practical for real-world applications. The Caputo derivative of order α, where $0 < \alpha \leqslant 1$, for a function $f(t)$ is defined as:

$$ {}_0D_t^{\alpha} f(t) = \frac{1}{\Gamma(1-\alpha)} \int_0^t \frac{f'(u)}{(t-u)^{\alpha}} du. \tag{13} $$

Here, $\Gamma(\cdot)$ is the Gamma function, and $f'(u)$ is the classical first-order derivative of $f(u)$. Table 1 lists a detailed description of the parameters used in both the integer-order and fractional-order SIR-SI models.

Theorem 2.1 The closed region $D = \{(x, y, z) \in \mathbb{R}_+{}^3;\ 0 \leq x + y \leq 1,\ 0 \leq z \leq 1\}$ is positively invarient set for model (12).

Proof Based on the model system given in Eq. (12), we obtain the following:

$$ x(t) + y(t) = 1 - \frac{R_h(t)}{N_h}, $$
$$ z(t) = 1 - \frac{S_v}{N_v}. $$

Thus, the model system (12) is bounded. □

Stability analysis

Equilibrium point

The model admits two categories of equilibrium points: the disease-free equilibrium (DFE) and the endemic equilibrium. According to model (12), we perform calculations on both points for the model.

The DFE occurs when there is no infection in the population, i.e., $y = 0$ and $z = 0$. The DFE point (E_1) of the model system (12) can be calculated by putting ${}_0D_t^{\kappa} x(t) = 0$, ${}_0D_t^{\kappa} y(t) = 0$, and ${}_0D_t^{\kappa} z(t) = 0$ and is given as $E_1 = (x_{eq}, y_{eq}, z_{eq}) = (1, 0, 0)$.

The endemic equilibrium point occurs when there is infection in the population. The endemic equilibrium point (E_2) of the model system (12) can be calculated by putting ${}_0D_t^{\kappa} x(t) = 0$, ${}_0D_t^{\kappa} y(t) = 0$, and ${}_0D_t^{\kappa} z(t) = 0$ and is given as

$$ E_2 = (x^*, y^*, z^*) = \left(\frac{\mu\gamma + \delta\alpha}{\delta(\alpha+\beta)}, \frac{\alpha(\delta\beta)}{\gamma\delta(\alpha+\beta)}, \frac{\alpha(\delta\beta - \mu\gamma)}{\beta(\mu\gamma + \delta\alpha)} \right) $$

.

Reproduction number

The compartments of the model (12) that are infected are made up of classes that exist in the (y, z) coordinates. Using the next generation technique[43,44], it is possible to compute the basic reproduction number R_0 by utilizing the relation $R_0 = \rho(FV^{-1})$, which represents the spectral radius of the eigenvalue of the Jacobian matrix evaluated at the DFE point E_1. Both the Jacobian matrix of the transmission terms, denoted by F, and the Jacobian matrix of the transition terms, represented by V, the values of which are, respectively,

$$ F = \begin{pmatrix} 0 & \beta \\ 0 & 0 \end{pmatrix} \quad \text{and} \quad V = \begin{pmatrix} \gamma & 0 \\ -\delta & \mu \end{pmatrix}. $$

Thus, the next generation matrix is written by:

$$ FV^{-1} = \begin{pmatrix} \frac{\delta\beta}{\gamma\mu} & \frac{\beta}{\mu} \\ 0 & 0 \end{pmatrix}. $$

The basic reproduction number (R_0) is the spectral radius of the eigenvalues of matrix FV^{-1}:

$$ R_0 = \rho(FV^{-1}) = \frac{\delta\beta}{\gamma\mu}. \tag{14} $$

Remark 3.1 The R_0, represents the expected number of secondary infections generated by a single infective individual in a fully susceptible population. It serves as a critical measure of disease spread potential and acts as a threshold for the stability of the DFE, aiding in disease control strategies.

Local and global stability of DFE

In numerous epidemiological models, a DFE exists, representing a state where the population is disease-free. The theorems below address the local and global stability of the DFE, denoted as E_1.

Theorem 3.1 The DFE of the model system described in Eq. (12) is locally asymptotically stable if $R_0 < 1$, and becomes unstable when $R_0 > 1$.

Proof : The local stability of the disease-free equilibrium point (E_1) is determined by analyzing the eigenvalues of the Jacobian matrix (J) evaluated at E_1:

$$J = \begin{pmatrix} -\alpha & 0 & -\beta \\ \beta z & -\gamma & \beta \\ 0 & \delta & -\mu \end{pmatrix}.$$

It is obvious that $\lambda_1 = -\alpha$ are first negative eigenvalues of *J*. The remaining eigenvalues of *J* are determined using the following block matrix (J_1), which helps analyze the system's stability and behavior. The matrix is

$$J_1 = \begin{pmatrix} -\gamma & \beta \\ \delta & -\mu \end{pmatrix}.$$

The characteristic equation associated with the matrix *J* is expressed a

$$P(\lambda) = \lambda^2 + (\gamma + \mu)\lambda + (\mu\gamma - \beta\delta).$$

By the Routh–Hurwitz-criteria[45] of stability and some algebraic manipulations, it can easily be proved that if $R_0 < 1$. Consequently, the Jacobian matrix (J_1) has negative real components in all of its eigenvalues. Hence, the disease-free equilibrium (DFE) of the model system (12) is locally asymptotically stable if $R_0 < 1$, and becomes unstable when $R_0 > 1$. □

The following theorem investigates the DFE's global stability using the approach developed by Castillo-Chavez and Song[46].

Theorem 3.2 If $R_0 < 1$, the DFE E_1 of the model (12) is globally asymptotically stable in its feasible region.

Proof We begin by reformulating the model (12) as follows:

$$\begin{aligned} {}_0D_t^{\kappa} X(t) &= F(X, Y), \\ {}_0D_t^{\kappa} Y(t) &= G(X, Y), \quad \text{with } G(X, 0) = 0, \end{aligned}$$

where the non-disease and disease compartments are represented as $X = x \in \mathbb{R}$ and $Y = (y, z) \in \mathbb{R}^2$ respectively. The subsequent two requirements (H_1) and (H_2) are necessary for the global asymptotic stability of the DFE of the model (12).

(H_1): For the system ${}_0D_t^{\kappa} X(t) = F(X, 0)$, the equilibrium point $X^* = x_{eq}$ is globally asymptotically stable, where $F(X^*, 0) = 0$.

(H_2): The function $G(X, Y)$ is expressed as $G(X, Y) = BY - G_1(X, Y)$, where $G_1(X, Y) \geq 0$ for all $(X, Y) \in D$, and $B = D_Y G(X^*, 0)$ is assumed to be an M-matrix. The non-negative off-diagonal entries of B guarantee that the system remains biologically meaningful within the region D.

For model (12), we have

$${}_0D_t^{\kappa} X(t) = F(X, 0) = \alpha(1 - x). \tag{15}$$

Indeed, the system (15) is globally asymptotically stable around $X^* = x_{eq} = 1$. This can be verified from the solution $x(t) = 1 - (1 - x_0)e^{-\alpha t}$ such that $\lim_{t \to \infty} x(t) = 1$, which implies that the global convergence of system (15) in *D*. Furthermore, from the model (12), we obtain

$$B = \begin{pmatrix} \gamma & \beta \\ \delta & -\mu \end{pmatrix}$$

and

$$G_1(X, Y) = \begin{pmatrix} \beta xz \\ 0 \end{pmatrix}.$$

Clearly, $\beta xz \geq 0$ inside *D* and therefore, $G_1(X, Y) \geq 0$. Thus, the two conditions (H_1) and (H_2) are satisfied. Therefore, the DFE E_1 of model (12) is globally asymptotically stable when $R_0 < 1$. □

Existence and uniqueness conditions of solution

In recent years, numerous studies have explored the existence and uniqueness of solutions for initial and boundary value problems related to NFDEs[47–49], contributing significantly to the theoretical development of fractional calculus and its applications. The model delineated in Eq. (12) can be articulated as follows:

$$\left.\begin{aligned} {}_0D_t^{\kappa} x(t) &= f_1(x(t), y(t), z(t)), \\ {}_0D_t^{\kappa} y(t) &= f_2(x(t), y(t), z(t)), \\ {}_0D_t^{\kappa} z(t) &= f_3(x(t), y(t), z(t)), \end{aligned}\right\}, t \geq 0, \ \kappa \in (0, 1],$$

with $x(0) = x_0$, $y(0) = y_0$, and $z(0) = z_0$ over the domain $\Omega = \{x(t), y(t), z(t) \in \mathbb{R} : |x(t)| \leq A_1, |y(t)| \leq A_2, |z(t)| \leq A_3, \ t \in [0, \rho]\}$. If $|f_i(x(t), y(t), z(t))| \leq M_i, \ i = 1, 2, 3$, and

$$\left|\frac{\partial f_i(x,y,z)}{\partial x}\right| \leq p_{1i}, \ \left|\frac{\partial f_i(x,y,z)}{\partial y}\right| \leq p_{2i}, \text{ and } \left|\frac{\partial f_i(x,y,z)}{\partial z}\right| \leq p_{3i}$$

then model (12) has the unique solution. The parameters M_i, A_i, p_{1i}, p_{2i}, and p_{3i}, $i = 1, 2, 3$ are positive constants.

Numerical procedure of SIR-SI model

A numerical technique utilizing the Caputo operator has been presented for modeling both nonlinear and linear systems, as previously identified by researchers[50]. Consequently, we now examine an IVP involving FO differential operators. We additionally construct a numerical approach utilizing Caputo derivatives to generate numerical estimates for models with both nonlinear and linear components[50]. The IVP involving the Caputo operator can be expressed as follows.

$$\begin{cases} {}_0D_t^{\kappa} \mathrm{b}(t) = P(t, \mathrm{b}(t)), \\ \mathrm{b}(0) = \mathrm{b}_0 \end{cases} \tag{16}$$

Fractional calculus is applied to derive the integral from the above equation, resulting in:

$$\mathrm{b}(t) - \mathrm{b}(0) = \frac{1}{\Gamma(k)} \int_0^t P(\tau, \mathrm{b}(\tau))(t-\tau)^{k-1} d\tau. \tag{17}$$

At the point, $t_{l+1} = (l+1)\Delta t, l = 0, 1, 2, \ldots$, from above equation can be written as

$$\mathrm{b}(t_{l+1}) - \mathrm{b}(0) = \frac{1}{\Gamma(k)} \int_0^{t_{l+1}} P(\tau, \mathrm{b}(\tau))(t_{l+1}-\tau)^{k-1} d\tau, \tag{18}$$

and we have

$$\mathrm{b}(t_{l+1}) - \mathrm{b}(0) = \frac{1}{\Gamma(k)} \sum_{m=0}^{l} \int_{t_m}^{t_{m+1}} P(\tau, \mathrm{b}(\tau))(t_{l+1}-\tau)^{k-1} d\tau. \tag{19}$$

To facilitate the simplification of the integral on the R.H.S. of Eq. (19), we insert the Lagrange polynomial into the equation:

$$\begin{aligned} \mathrm{b}^{l+1} = \mathrm{b}_0 + \frac{1}{\Gamma(k)} \sum_{m=0}^{l} \int_{t_m}^{t_{m+1}} \Big[\frac{P(t_m, \mathrm{b}^m)}{\Delta t}(\tau - t_{m-1}) \\ fracP(t_{m-1}, \mathrm{b}^{m-1})\Delta t(\tau - t_m) \Big] \times (t_{l+1} - \tau)^{k-1} d\tau. \end{aligned} \tag{20}$$

Thus, Eq. (20) can be reconstructed as follows:

$$\begin{aligned} \mathrm{b}^{l+1} = \mathrm{b}_0 + \frac{1}{\Gamma(k)} \sum_{m=0}^{l} \Big[\int_{t_m}^{t_{m+1}} \frac{P(t_m, \mathrm{b}^m)}{\Delta t}(\tau - t_{m-1}) \times (t_{l+1} - \tau)^{k-1} d\tau \\ int_{t_m}^{t_{m+1}} \frac{P(t_{m-1}, \mathrm{b}^{m-1})}{\Delta t}(\tau - t_m) \times (t_{l+1} - \tau)^{k-1} d\tau \Big], \end{aligned} \tag{21}$$

and we have

$$\begin{aligned} \mathrm{b}^{l+1} = \mathrm{b}_0 + \frac{1}{\Gamma(k)} \sum_{m=0}^{l} \frac{P(t_m, \mathrm{b}^m)}{\Delta t} \int_{t_m}^{t_{m+1}} (\tau - t_{m-1}) \times (t_{l+1} - \tau)^{k-1} d\tau \\ frac1\Gamma(k) \sum_{m=0}^{l} \frac{P(t_{m-1}, \mathrm{b}^{m-1})}{\Delta t} \int_{t_m}^{t_{m+1}} (\tau - t_m) \times (t_{l+1} - \tau)^{k-1} d\tau. \end{aligned} \tag{22}$$

The integrals in Eq. (22) are computed as follows:

$$\begin{aligned}
&\int_{t_m}^{t_{m+1}} (\tau - t_{m-1}) \times (t_{l+1} - \tau)^{k-1} d\tau \\
&= \frac{\Delta t)^{k+1}}{k(k+1)} \Big[(l-m+1)^k (l-m+k+2) - (l-m)^k (l-m+2k+2) \Big] \\
&\int_{t_m}^{t_{m+1}} (\tau - t_m) \times (t_{l+1} - \tau)^{k-1} d\tau \\
&= \frac{\Delta t)^{k+1}}{k(k+1)} \Big[(l-m+1)^{k+1} - (l-m)^k (l-m+k+1) \Big]
\end{aligned} \tag{23}$$

Inserting the value of these integrals in Eq. (22), we obtain

$$\begin{aligned}
\mathrm{b}^{l+1} = \mathrm{b}_0 + \frac{(\Delta t)^k}{\Gamma(k+2)} \sum_{m=0}^{l} P(t_m, \mathrm{b}^m) \Big[(l-m+1)^k (l-m+k+2) - (l-m)^k (l-m+2k+2) \Big] \\
frac(\Delta t)^k \Gamma(k+2) \sum_{m=0}^{l} P(t_{m-1}, \mathrm{b}^{m-1}) \Big[(l-m+1)^{k+1} - (l-m)^k (l-m+k+1) \Big].
\end{aligned} \tag{24}$$

Similarly, Eq. (12) can be obtained the numerical solution as follows:

$$\begin{aligned}
x^{l+1} = x_0 + \frac{(\Delta t)^k}{\Gamma(k+2)} \sum_{m=0}^{l} P_1(t_m, x^m, y^m, z^m) \Big[(l-m+1)^k (l-m+k+2) - (l-m)^k (l-m+2k+2) \Big] \\
frac(\Delta t)^k \Gamma(k+2) \sum_{m=0}^{l} P(t_{m-1}, x^{m-1}, y^{m-1}, z^{m-1}) \Big[(l-m+1)^{k+1} - (l-m)^k (l-m+k+1) \Big].
\end{aligned} \tag{25}$$

$$\begin{aligned}
y^{l+1} = y_0 + \frac{(\Delta t)^k}{\Gamma(k+2)} \sum_{m=0}^{l} P_1(t_m, x^m, y^m, z^m) \Big[(l-m+1)^k (l-m+k+2) - (l-m)^k (l-m+2k+2) \Big] \\
frac(\Delta t)^k \Gamma(k+2) \sum_{m=0}^{l} P(t_{m-1}, x^{m-1}, y^{m-1}, z^{m-1}) \Big[(l-m+1)^{k+1} - (l-m)^k (l-m+k+1) \Big].
\end{aligned} \tag{26}$$

$$\begin{aligned}
z^{l+1} = z_0 + \frac{(\Delta t)^k}{\Gamma(k+2)} \sum_{m=0}^{l} P_1(t_m, x^m, y^m, z^m) \Big[(l-m+1)^k (l-m+k+2) - (l-m)^k (l-m+2k+2) \Big] \\
frac(\Delta t)^k \Gamma(k+2) \sum_{m=0}^{l} P(t_{m-1}, x^{m-1}, y^{m-1}, z^{m-1}) \Big[(l-m+1)^{k+1} - (l-m)^k (l-m+k+1) \Big].
\end{aligned} \tag{27}$$

Sensitivity analysis of the parameters

The aim of conducting a sensitivity analysis for an epidemic model is to identify the parameters that are most important about a particular intervention that significantly impacts the dynamics of the disease situation. We are interested in the features that are responsible for the significant variance in the value of the fundamental reproduction number. When a parameter is changed, the sensitivity indices can be utilized to ascertain the equivalent variation in the state variable that is brought about by the modification. For the purpose of calculating these indices, the definition provided in[51] was utilized. The ratio between the relative change in the variable and parameter is known as normalized forward sensitivity index. When the variable in question is a parameter function that can be differentiated, the sensitivity index is computed by employing partial derivatives. The normalized forward sensitivity index of a variable, represented by R_0, with respect to a parameter p, is defined as the relative change in R_0 resulting from a relative change in p:

$$S_p^{R_0} = \frac{p}{R_0} \frac{\partial R_0}{\partial p}.$$

Using the basic reproduction number (R_0 from Eq. (14)), we conduct a sensitivity analysis to identify the most influential parameters of the model. The sensitivity index for the parameters (β, δ, γ, and μ) can be calculated as follows:

$$S_\beta^{R_0} = \frac{\beta}{R_0} \frac{\partial R_0}{\partial \beta} = 1, \quad S_\delta^{R_0} = \frac{\delta}{R_0} \frac{\partial R_0}{\partial \delta} = 1, \quad S_\gamma^{R_0} = \frac{\gamma}{R_0} \frac{\partial R_0}{\partial \gamma} = -1, \quad S_\mu^{R_0} = \frac{\mu}{R_0} \frac{\partial R_0}{\partial \mu} = -1. \tag{28}$$

The parameters (β and δ) with positive indices in Eq. (28) increase the value of R_0, indicating a rise in disease transmission within the population. Conversely, parameters (γ and μ) with negative indices suggest a reduction in disease infection. As shown in Eq. (28), the most significant positive indices parameters are β and δ. This indicates that β and δ are the most sensitive parameters with positive indices, implying that controlling these

values can effectively reduce R_0. Furthermore, the parameters with the most significant negative indices are γ and μ. This indicates that γ and μ are the most sensitive parameters with negative indices, implying that controlling these values can effectively reduce R_0. Raising awareness about *beta*, *delta*, γ, and μ within the population could help manage the transmission of dengue fever. Figure 2 depicts the parameters' sensitivity analysis.

Numerical results and discussion

The parameter values and the initial population values are taken from[41,42]: $\alpha = 0.00004$, $\beta = 0.009191$, $\gamma = 0.3333, \delta = 0.375, \mu = 0.083333, x(0) = 0.9999, y(0) = 0.0006$, and $z(0) = 0.056$. Table 2 presents the numerical solutions obtained for $x(t)$, $y(t)$, and $z(t)$, together with the corresponding reference values reported in[52] for Case I. This table also includes the respective absolute errors, denoted by E_x, E_y, and E_z, thereby providing a direct quantitative comparison between the computed and reference results. The close agreement between the two sets of results attests to the high accuracy of the proposed method, thereby demonstrating its robustness and effectiveness in producing reliable numerical approximations. Figure 3 illustrates the behavior of the present model for different fractional orders: $k = 0.70, 0.80, 0.90$, and 1.00. The number of susceptible and infected individuals for humans, as well as infected mosquitoes, increases as the fractional order value decreases. Furthermore, $x(t)$ decreases as time progresses, but after 50 days, $x(t)$, $y(t)$, and $z(t)$ stabilize. From Fig. 3b, we observe that the initially infected population increases with time, then decreases after a certain period and stabilizes after 150 days. Figure 4 depicts the combined plotting of the solution of the present model for fractional orders $k = 0.10, 0.30$, and 0.50. Figure 5 illustrates the chaotic behavior of the present model for distinct fractional order values $k = 0.70, 0.80, 0.90$, and 1.00. Figure 6 displays the effect of the parameter β on the behavior of the present model (12) for fractional orders $\kappa = 0.90$ and 1.00. It can be observed that the susceptible population decreases as the parameter β increases for values $\beta = 0.001, 0.002, 0.003$, and 0.004, whereas the infected and recovered populations increase for these values of β (see Figure 6). Figure 7 illustrates the effect of the parameter δ on the behavior of the present model (12) for fractional orders $\kappa = 0.90$ and 1.00. Similar to β, the susceptible population decreases as δ increases for values $\delta = 0.001, 0.002, 0.003$, and 0.004, whereas the infected and recovered populations increase for these values (see Fig. 7). Figure 8 portraits the effect of the parameter μ on the behavior of the present model (12) for fractional orders $\kappa = 0.90$ and 1.00.

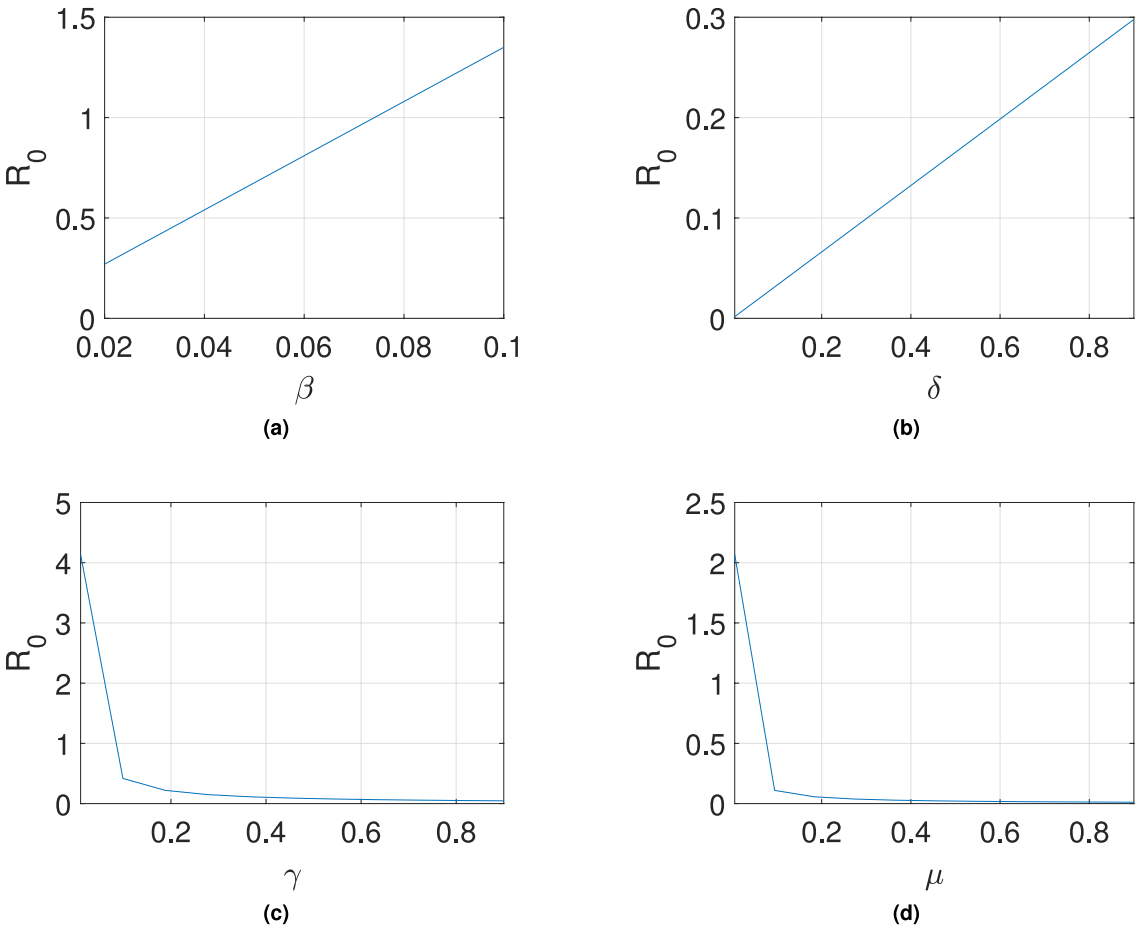

Fig. 2. Analysis of the sensitivity of the basic reproduction number R_0 with respect to different model parameters.

t	$x(t)$	$x(t)$[52]	E_x	$y(t)$	$y(t)$[52]	E_y	$z(t)$	$z(t)$[52]	E_z
0.0	0.9999000000	0.9999000000	0	0.0000460000	0.0000460000	0	0.0560000000	0.0560000000	0
0.1	0.9986673191	0.9986025092	6.48e−5	0.0012755922	0.0013383237	6.27e−5	0.0558511089	0.05584432375	6.79e−6
0.2	0.9973744401	0.9973097660	6.47e−5	0.0025061690	0.0025668085	6.06e−5	0.0557379906	0.05573333080	4.66e−6
0.3	0.9960853554	0.9960206778	6.47e−5	0.0036932091	0.0037521427	5.89e−5	0.0556679721	0.05566517284	2.80e−6
0.4	0.9947990780	0.9947341552	6.49e−5	0.0048390916	0.0048970106	5.79e−5	0.0556394191	0.05563800157	1.42e−6
0.5	0.9935146630	0.9934491131	6.55e−5	0.0059460778	0.0060040922	5.80e−5	0.0556507790	0.05564996870	8.10e−7
0.6	0.9922312050	0.9921644705	6.67e−5	0.0070163166	0.0070760632	5.97e−5	0.0557005773	0.05569922591	1.35e−6
0.7	0.9909478363	0.9908791497	6.87e−5	0.0080518503	0.0081155951	6.37e−5	0.0557874143	0.05578392491	3.49e−6
0.8	0.9896637251	0.9895920774	7.16e−5	0.0090546198	0.0091253552	7.07e−5	0.0559099613	0.05590221740	7.74e−6
0.9	0.9883780738	0.9883021840	7.59e−5	0.0100264698	0.0101080063	8.15e−5	0.0560669575	0.05605225506	1.47e−5
1.0	0.9870901169	0.9870084040	8.17e−5	0.0109691535	0.0110662072	9.71e−5	0.0562572067	0.05623218960	2.50e−5

Table 2. Comparison of the numerical solutions $x(t)$, $y(t)$, and $z(t)$ obtained using the present method with those reported in[52] for case-I, including the corresponding absolute errors.

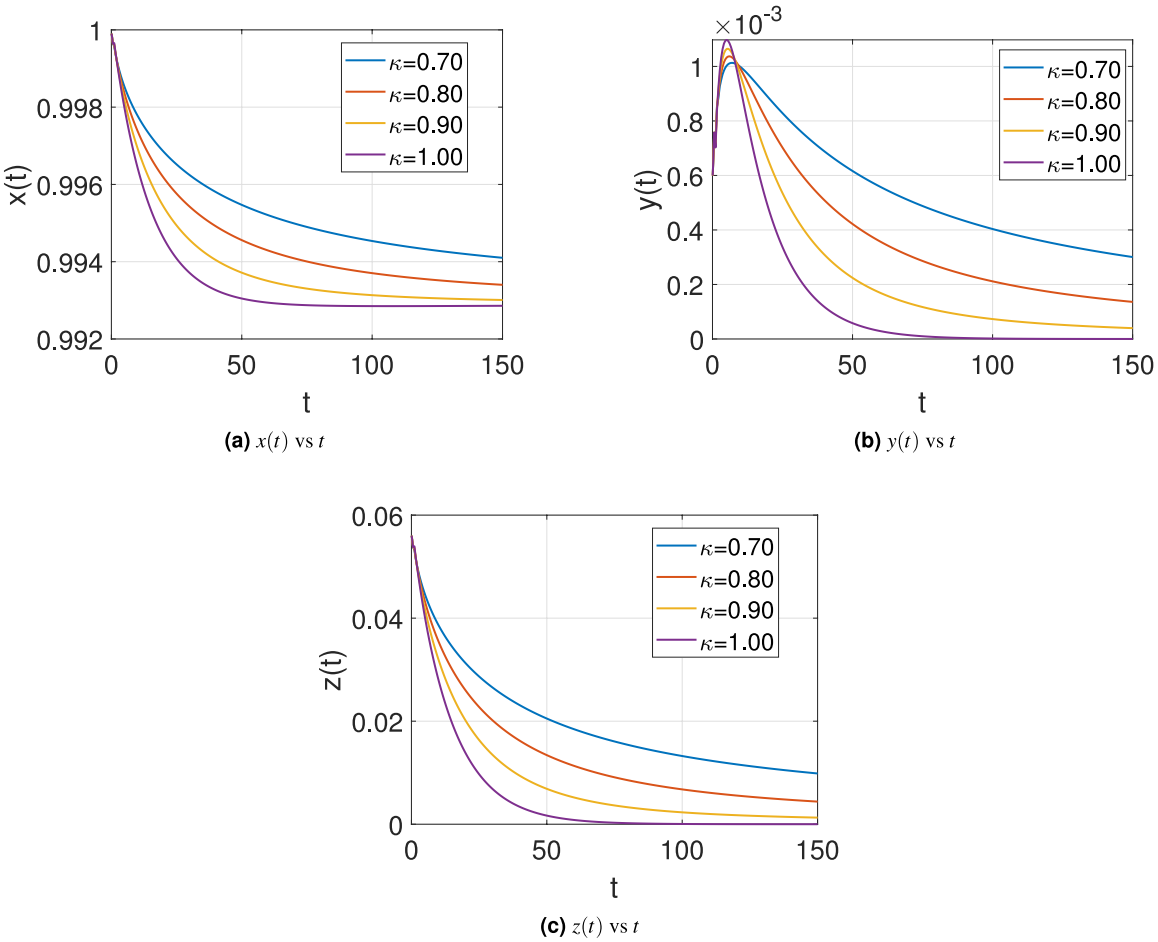

(a) $x(t)$ vs t **(b)** $y(t)$ vs t **(c)** $z(t)$ vs t

Fig. 3. Behavior of the proposed model (12) for distinct values of fractional order (κ).

It is evident that the susceptible population increases as μ increases ($\mu = 0.03, 0.05, 0.07, 0.09$), whereas the infected and recovered populations decrease with increasing μ (see Figure 8). Figure 9 shows the effect of the parameter γ on the behavior of the present model (12) for fractional orders $\kappa = 0.90$ and 1.00. The susceptible population increases as γ increases ($\gamma = 0.01, 0.02, 0.03, 0.04$), while the infected and recovered populations decrease with increasing γ (see Fig. 9).

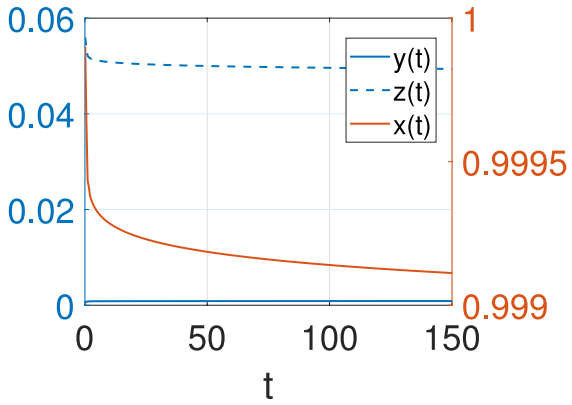

(a) For $\kappa = 0.10$

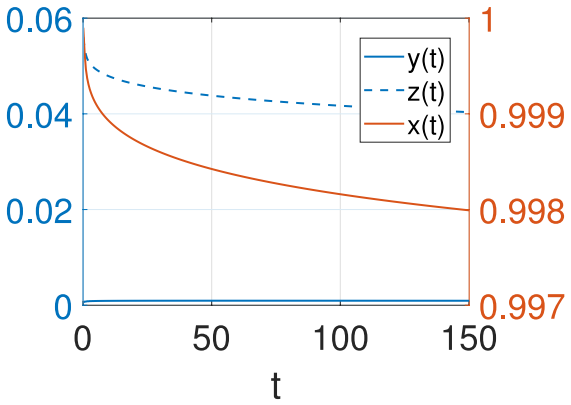

(b) For $\kappa = 0.30$

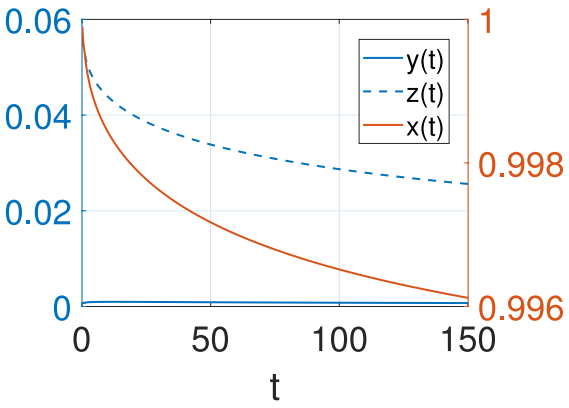

(c) For $\kappa = 0.50$

Fig. 4. Combine ploting of the solution of the present model (12) for fractional order ($\kappa = 0.10, 0.30$, and 0.50).

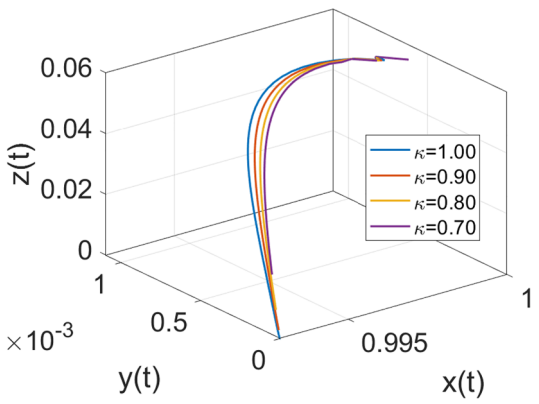

Fig. 5. Chaotic behaviour of the present model (12) for distinct values of fractional order (κ).

Conclusion

This study employed the Caputo fractional derivative to investigate the epidemic dynamics of a SIR-SI model. Numerical techniques were implemented to solve the proposed system. Both the disease-free and endemic equilibrium points were explored, and a comprehensive analysis of local and global stability at the disease-free equilibrium was conducted. Additionally, a sensitivity analysis of parameters β, δ, μ, and γ was conducted concerning the basic reproduction number R_0. The conditions for the existence and uniqueness of the solution within a stable framework were established. Numerical simulations supported the theoretical findings, showing that the fractional-order model exhibited a lower peak of infection, aligning more accurately with empirical

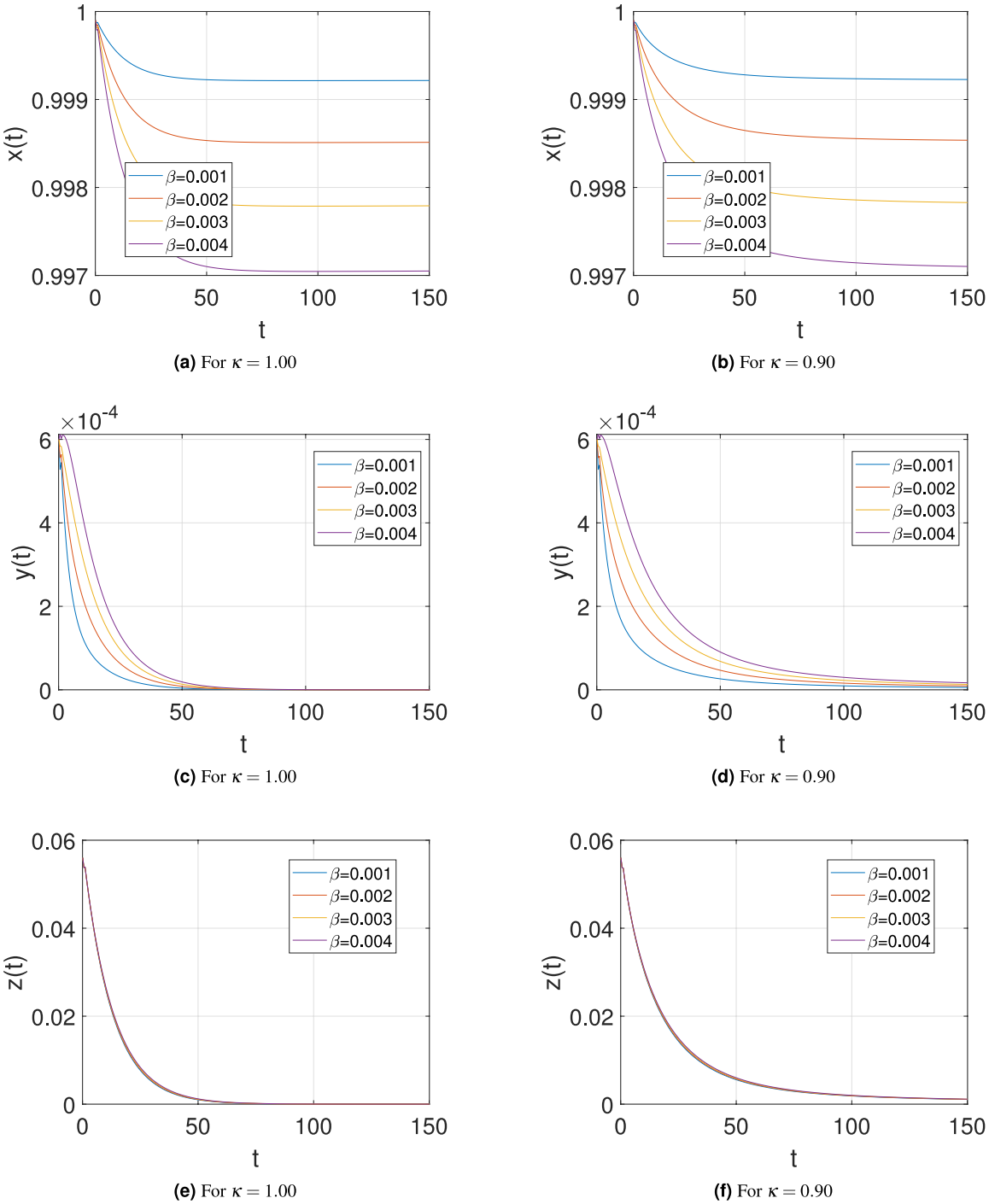

(a) For $\kappa = 1.00$ **(b)** For $\kappa = 0.90$

(c) For $\kappa = 1.00$ **(d)** For $\kappa = 0.90$

(e) For $\kappa = 1.00$ **(f)** For $\kappa = 0.90$

Fig. 6. Effect of parameter (β) on the behavior of the present model (12) for fractional order ($\kappa = 0.90$ and 1.00).

data. The impact of varying parameter values on the model's outcomes was discussed. Fractional mathematical modeling demonstrated a more precise and resilient approach for epidemiological models by utilizing fractional orders that closely matched real-world data. The fractional SIR-SI model can be expanded in future studies by adding other dengue serotypes, climate variables, and actual data. Stochastic or spatial dynamics and time-dependent fractional orders could enhance realism. These developments can improve forecasting precision and facilitate better public health strategies for preventing dengue fever outbreaks.

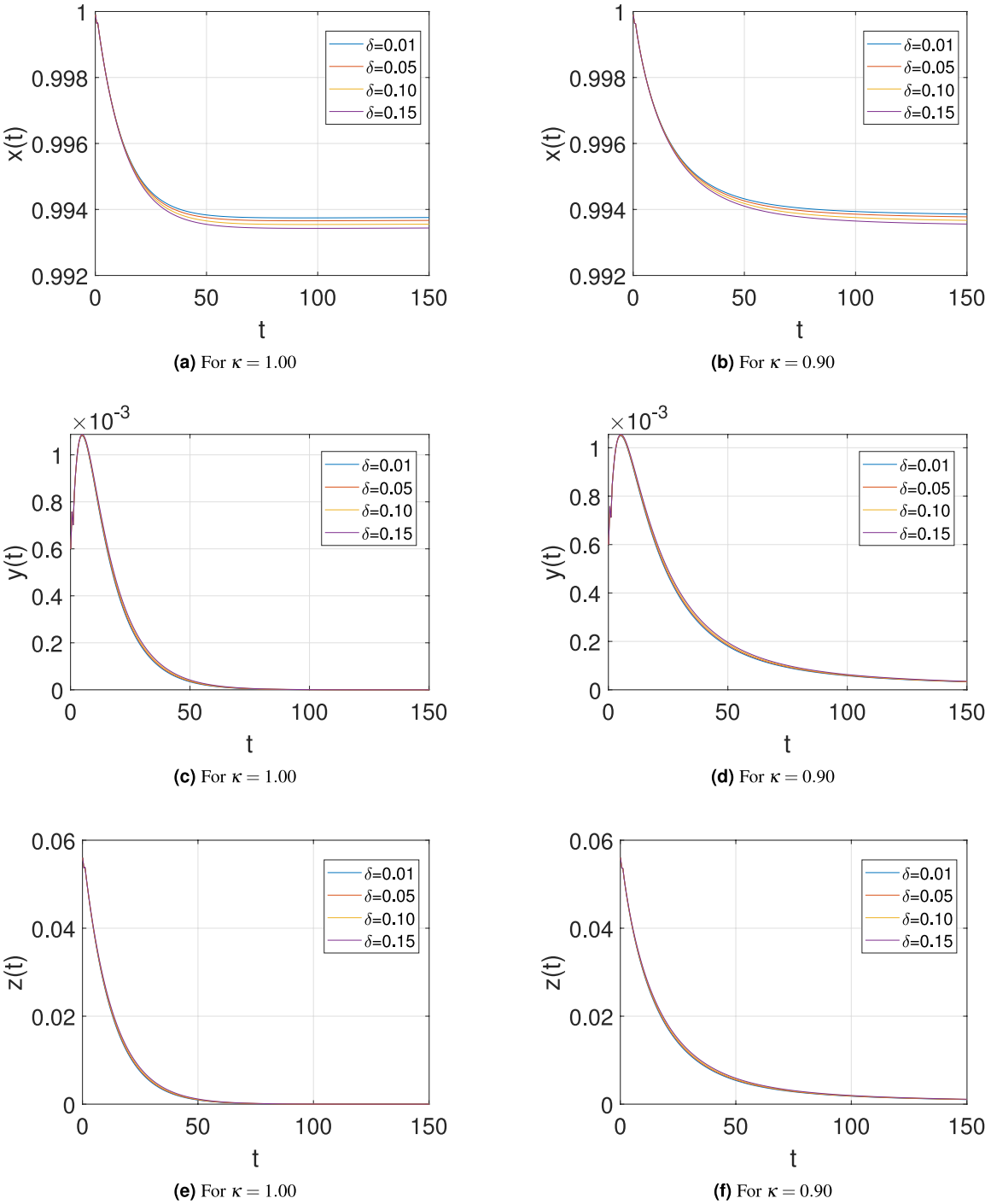

(a) For $\kappa = 1.00$ **(b)** For $\kappa = 0.90$

(c) For $\kappa = 1.00$ **(d)** For $\kappa = 0.90$

(e) For $\kappa = 1.00$ **(f)** For $\kappa = 0.90$

Fig. 7. Effect of parameter (δ) on the behaviour of the present model (12) for fractional order ($\kappa = 0.90$ and 1.00).

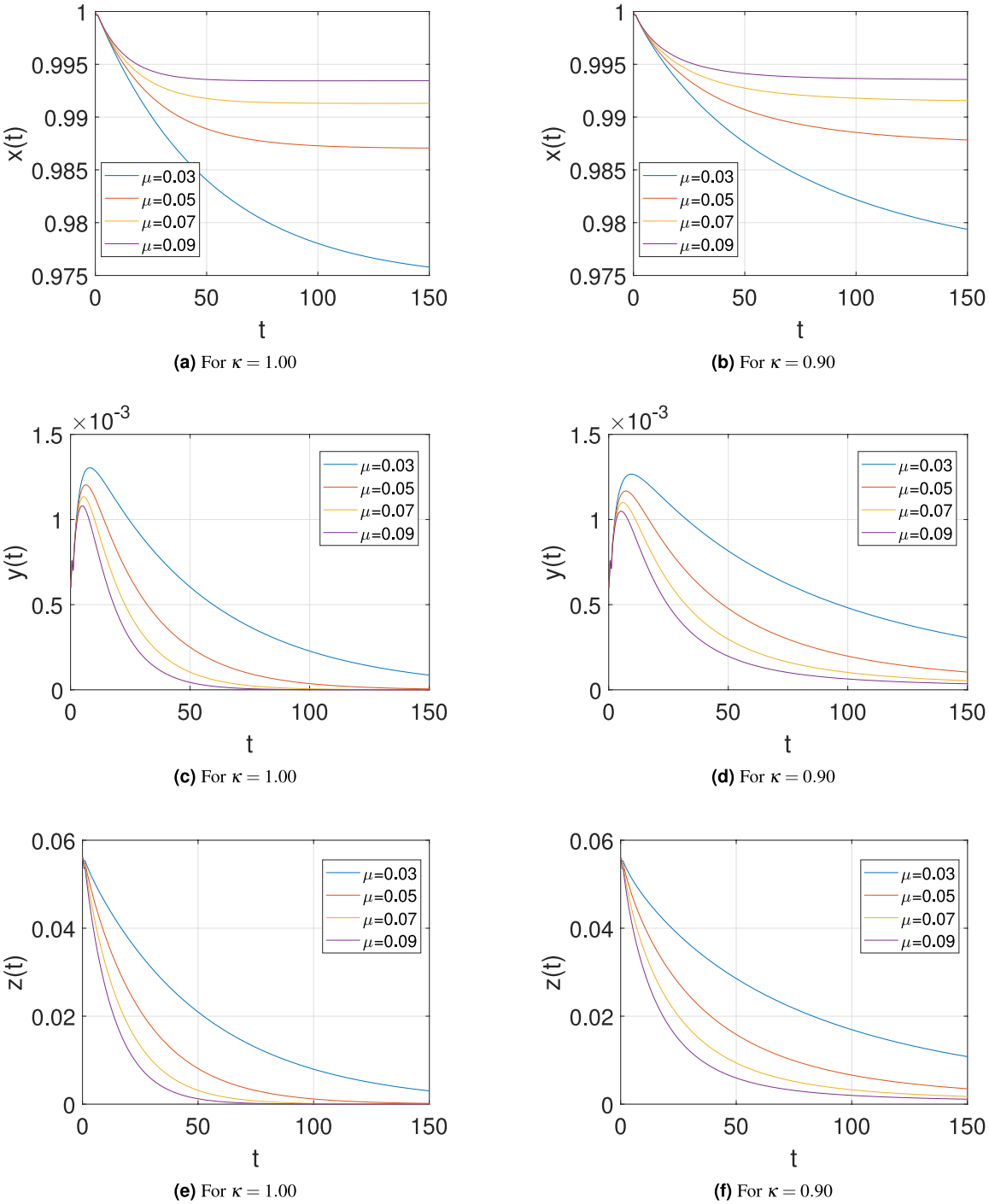

(a) For $\kappa = 1.00$ **(b)** For $\kappa = 0.90$

(c) For $\kappa = 1.00$ **(d)** For $\kappa = 0.90$

(e) For $\kappa = 1.00$ **(f)** For $\kappa = 0.90$

Fig. 8. Effect of parameter (μ) on the behavior of the present model (12) for fractional order ($\kappa = 0.90$ and 1.00).

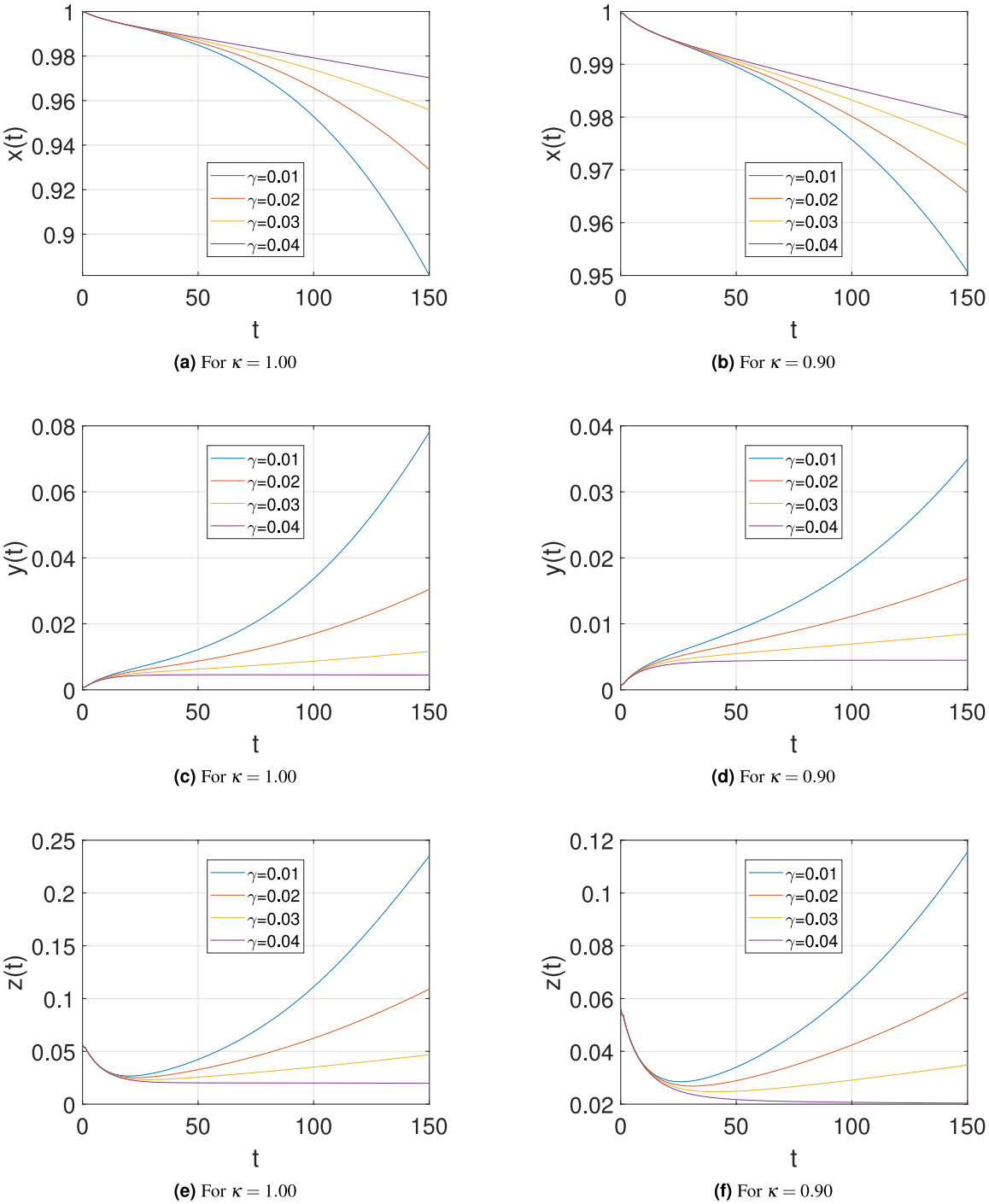

(a) For $\kappa = 1.00$ **(b)** For $\kappa = 0.90$

(c) For $\kappa = 1.00$ **(d)** For $\kappa = 0.90$

(e) For $\kappa = 1.00$ **(f)** For $\kappa = 0.90$

Fig. 9. Effect of parameter (γ) on the behaviour of the present model (12) for fractional order ($\kappa = 0.90$ and 1.00).

Data availability

The data sets used and/or analyzed during the current study available from the corresponding author on reasonable request.

Received: 30 March 2025; Accepted: 18 August 2025
Published online: 21 August 2025

References

1. Kularatne, S. A. Dengue fever. *BMJ* **351** (2015).

2. W. H. Organization, Fact sheets: Dengue and dengue haemorrhagic fever. https://www.who.int/news-room/fact-sheets/detail/dengue-and-severe-dengue. Accessed 13 Jan 2024 (2015).
3. Sanusi, W. et al. Analysis and simulation of SIRS model for dengue fever transmission in South Sulawesi, Indonesia. *J. Appl. Math.* **2021**(1), 2918080 (2021).
4. Omame, A., Rwezaura, H., Diagne, M., Inyama, S. & Tchuenche, J. Covid-19 and dengue co-infection in Brazil: Optimal control and cost-effectiveness analysis. *Eur. Phys. J. Plus.* **136**(10), 1090 (2021).
5. Iheonu, N., Nwajeri, U. & Omame, A. A non-integer order model for zika and dengue co-dynamics with cross-enhancement. *Healthc. Anal.* **4**, 100276 (2023).
6. Usman, M., Abbas, M., Khan, S. H. & Omame, A. Analysis of a fractional-order model for dengue transmission dynamics with quarantine and vaccination measures. *Sci. Rep.* **14**(1), 11954 (2024).
7. Esteva, L. & Vargas, C. Analysis of a dengue disease transmission model. *Math. Biosci.* **150**(2), 131–151 (1998).
8. Chanprasopchai, P., Tang, I. M. & Pongsumpun, P. SIR model for dengue disease with effect of dengue vaccination. *Comput. Math. Methods Med.* **2018**(1), 9861572 (2018).
9. Supriatna, A. K. et al. Age-dependent survival rates in SIR-SI dengue transmission model and its application considering human vaccination and wolbachia infection in mosquitoes. *Mathematics* **10**(21), 3950 (2022).
10. Luo, M., Qiu, W., Nikan, O. & Avazzadeh, Z. Second-order accurate, robust and efficient ADI Galerkin technique for the three-dimensional nonlocal heat model arising in viscoelasticity. *Appl. Math. Comput.* **440**, 127655 (2023).
11. Nikan, O., Tenreiro Machado, J. A., Golbabai, A. & Rashidinia, J. Numerical evaluation of the fractional Klein-Kramers model arising in molecular dynamics. *J. Comput. Phys.* **428**, 109983 (2021).
12. Molavi-Arabshahi, M., Rashidinia, J. & Yousefi, M. A novel hybrid method with convergence analysis for approximation of HTLV-I dynamics model. *Sci. Rep.* **14**(1), 25678 (2024).
13. Nikan, O., Tenreiro Machado, J. A., Golbabai, A. & Nikazad, T. Numerical investigation of the nonlinear modified anomalous diffusion process. *Nonlinear Dyn.* **97**(4), 2757–2775 (2019).
14. Yaagoub, Z. Fractional two-strain SVLIR epidemic model with vaccination and quarantine strategies. *Int. J. Dyn. Control* **13**(2), 55 (2025).
15. Yaagoub, Z. & Allali, K. Fractional HBV infection model with both cell-to-cell and virus-to-cell transmissions and adaptive immunity. *Chaos Solitons Fract.* **165**, 112855 (2022).
16. Yaagoub, Z., Sadki, M. & Allali, K. A generalized fractional hepatitis B virus infection model with both cell-to-cell and virus-to-cell transmissions. *Nonlinear Dyn.* **112**(18), 16559–16585 (2024).
17. Maayah, B., Bushnaq, S. & Moussaoui, A. Numerical solution of fractional order SIR model of dengue fever disease via Laplace optimized decomposition method. *J. Math. Comput. Sci.* **32**(1), 86–93 (2024).
18. Prasad, R., Kumar, K. & Dohare, R. Caputo fractional order derivative model of Zika virus transmission dynamics. *J. Math. Comput. Sci.* **28**(2), 145–157 (2023).
19. Hajhouji, Z., Hattaf, K. & Yousfi, N. A generalized fractional HIV-1 infection model with humoral immunity and highly active antiretroviral therapy. *J. Math. Comput. Sci.* **32**(2), 160–174 (2024).
20. Kilicman, A. A fractional order SIR epidemic model for dengue transmission. *Chaos Solit. Fract.* **114**, 55–62 (2018).
21. Hamdan, N. I. & Kilicman, A. Analysis of the fractional order dengue transmission model: A case study in Malaysia. *Adv. Differ. Equ.* **2019**, 1–13 (2019).
22. Hoang, M. T., Zafar, Z. U. A. & Ngo, T. K. Q. Dynamics and numerical approximations for a fractional-order SIS epidemic model with saturating contact rate. *Comput. Appl. Math.* **39**, 1–20 (2020).
23. Ahmad, S. et al. Analysis and numerical solution of novel fractional model for dengue. *Results Phys.* **28**, 104669 (2021).
24. Harris, J. E. A tight fit of the sir dynamic epidemic model to daily cases of COVID-19 reported during the 2021–2022 omicron surge in New York City: A novel approach. *Stat. Methods Med. Res.* **33**(10), 1877–1898 (2024).
25. Contreras, S., Villavicencio, H. A., Medina-Ortiz, D., Biron-Lattes, J. P. & Olivera-Nappa, Á. A multi-group SEIRA model for the spread of COVID-19 among heterogeneous populations. *Chaos Solit. Fract.* **136**, 109925 (2020).
26. Medina-Ortiz, D., Contreras, S., Barrera-Saavedra, Y., Cabas-Mora, G. & Olivera-Nappa, Á. Country-wise forecast model for the effective reproduction number R_t of coronavirus disease. *Front. Phys.* **8**, 304 (2020).
27. Khan, T., Ullah, R., Alwan, B. A., El-Khatib, Y. & Zaman, G. Correlated stochastic epidemic model for the dynamics of SARS-CoV-2 with vaccination. *Sci. Rep.* **12**(1), 16105 (2022).
28. Khan, T., Rihan, F. A. & Al-Mdallal, Q. M. An epidemiological model for analysing pandemic trends of novel coronavirus transmission with optimal control. *J. Biol. Dyn.* **18**(1), 2299001 (2024).
29. Khan, T., Ahmad, S., Ullah, R., Bonyah, E. & Ansari, K. J. The asymptotic analysis of novel coronavirus disease via fractional-order epidemiological model. *AIP Adv.* **12**(3) (2022).
30. Sapakova, S., Sapakov, A. & Ipalakova, M. T. Using the SIR model to analyze the epidemiological situation in Kazakhstan and neighboring countries. In *Proceedings of the DTESI* (2022).
31. Mungkasi, S. Improved variational iteration solutions to the SIR model of dengue fever disease for the case of South Sulawesi. *J. Math. Fundam. Sci.* **52**(3) (2020).
32. Shah, K., Jarad, F. & Abdeljawad, T. On a nonlinear fractional order model of dengue fever disease under Caputo-Fabrizio derivative. *Alex. Eng. J.* **59**(4), 2305–2313 (2020).
33. Vijayalakshmi, G. & Ariyanatchi, M. Adams-Bashforth Moulton numerical approach on dengue fractional Atangana Baleanu Caputo model and stability analysis. *Int. J. Appl. Comput. Math.* **10**(1), 32 (2024).
34. Jan, R. & Boulaaras, S. Analysis of fractional-order dynamics of dengue infection with non-linear incidence functions. *Trans. Inst. Meas. Control.* **44**(13), 2630–2641 (2022).
35. Maayah, B., Bushnaq, S. & Moussaoui, A. Numerical solution of fractional order SIR model of dengue fever disease via Laplace optimized decomposition method. *J. Math. Comput. Sci.* **32**(1), 86–93 (2024).
36. Ahmad, R. et al. A new fractional-order stability analysis of SIR model for the transmission of Buruli disease: A biomedical application. *Fractals* **30**(05), 2240171 (2022).
37. Nisar, K. S., Farman, M., Abdel-Aty, M. & Ravichandran, C. A review of fractional order epidemic models for life sciences problems: Past, present and future. *Alex. Eng. J.* **95**, 283–305 (2024).
38. Sabir, Z., Raja, M. A. Z., Javeed, S. & Guerrero-Sanchez, Y. Numerical investigations of a fractional nonlinear dengue model using artificial neural networks. *Fractals* **30**(10), 2240241 (2022).
39. Meetei, M. Z., Zafar, S., Zaagan, A. A., Mahnashi, A. M. & Idrees, M. Dengue transmission dynamics: A fractional-order approach with compartmental modeling. *Fractal Fract.* **8**(4), 207 (2024).
40. Youssef, A. A. H. et al. An overview of some biomathematical models of dengue fever virus transmission. *Appl. Res. Sci. Humanit.* **1**(1), 1–22 (2024).
41. Diaz, J. P. Computational analysis of the SIR mathematical model for the dengue fever. (The University of Texas Rio Grande Valley, 2015).
42. El-shenawy, A., El-Gamel, M. & Teba, A. Simulation of the SIR dengue fever nonlinear model: A numerical approach. *Part. Differ. Equ. Appl. Math.* 100891 (2024).
43. Van den Driessche, P. & Watmough, J. Reproduction numbers and sub-threshold endemic equilibria for compartmental models of disease transmission. *Math. Biosci.* **180**(1–2), 29–48 (2002).

44. Diekmann, O., Heesterbeek, J. & Roberts, M. G. The construction of next-generation matrices for compartmental epidemic models. *J. R. Soc. Interface.* **7**(47), 873–885 (2010).
45. Allen, L. J. An Introduction to Mathematical Biology. (Pearson Prentice Hall, 2007).
46. Castillo-Chavez, C. & Song, B. Dynamical models of tuberculosis and their applications. *Math. Biosci. Eng.* **1**(2), 361–404 (2004).
47. Deng, J. & Ma, L. Existence and uniqueness of solutions of initial value problems for nonlinear fractional differential equations. *Appl. Math. Lett.* **23**(6), 676–680 (2010).
48. Den, J. & Deng, Z. Existence of solutions of initial value problems for nonlinear fractional differential equations. *Appl. Math. Lett.* **32**, 6–12 (2014).
49. Meena, R. K. & Kumar, S. A study on fractional SIR epidemic model with vital dynamics and variable population size using the residual power series method. *J. Comput. Anal. Appl.* **33**(1) (2024).
50. Atangana, A. & Araz, S. İ. New Numerical Scheme with Newton Polynomial: Theory, Methods, and Applications. (Academic Press, 2021).
51. Chitnis, N., Hyman, J. M. & Cushing, J. M. Determining important parameters in the spread of malaria through the sensitivity analysis of a mathematical model. *Bull. Math. Biol.* **70**, 1272–1296 (2008).
52. Rangkuti, Y. M., Side, S. & Noorani, M. S. M. Numerical analytic solution of sir model of dengue fever disease in South Sulawesi using homotopy perturbation method and variational iteration method. *J. Math. Fundam. Sci.* **46**(1), 91–105 (2014).

Acknowledgements

The authors express their heartfelt gratitude to the Editor and anonymous reviewers whose insightful comments and thoughtful recommendations significantly enhanced the overall quality of this work.

Author contributions

L Verma: Formal analysis (equal); Funding acquisition (equal); Investigation (equal); Software (equal); Supervision (equal); Writing-original draft (equal). R Meher: Data curation (equal); Resources (equal); Validation (equal). O Nikan: Investigation (equal); Writing–review & editing (equal). A.A Al-Saedi: Writing–review & editing (equal).

Declarations

Competing interests

The authors declare no competing interests.

Additional information

Correspondence and requests for materials should be addressed to O.N.

Reprints and permissions information is available at www.nature.com/reprints.

Publisher's note Springer Nature remains neutral with regard to jurisdictional claims in published maps and institutional affiliations.